Spectrally Discriminating Time-Resolved and Space-Resolved X-Ray Plasma Diagnostics

MARTIN C. RICHARDSON, SENIOR MEMBER, IEEE, ROBIN S. MARJORIBANKS, S. A. LETZRING, JAMES M. FORSYTH, AND DAVID M. VILLENEUVE

Abstract—**The experimental study of laser-produced plasmas, particularly those relevant to laser fusion, has long motivated the development of new X-ray plasma diagnostic techniques. This paper summarizes the application of a number of novel space-resolved and time-resolved X-ray diagnostic systems to the study of plasmas produced by the 1 beam 0.35 μm GDL facility, and by the 24 beam 1.05 μm OMEGA facility at the Laboratory for Laser Energetics. Two time-resolving X-ray spectrometers are described, one utilizing a transmission grating as a dispersive element, the other employing an array of K-edge filters for spectral discrimination. A transmission grating is also used in conjunction with a Kirkpatrick–Baez microscope to provide spectrally dispersed high spatial resolution images of the laser-produced plasmas. The usefulness of these instruments in measuring specific plasma parameters and identifying particular spectral features, in some cases with the aid of other diagnostic instrumentation, is illustrated.**

I. INTRODUCTION

EXAMINATION of the spectral characteristics of X-ray emission from high-density plasmas has long been utilized as an effective diagnostic of the plasma state. The diagnosis of laser-produced plasmas makes special requirements of X-ray spectroscopic techniques in that the extremes of temperature and density are created within microscopic regions and evolve in time on an ultrafast time scale. There is currently a strong interest in such plasmas, notably because of their utilization in various laser fusion [1] and X-ray laser schemes [2], but also because of a more general need to understand the rich variety of interaction mechanisms possible in such plasmas. In addition, laser-produced plasmas show considerable potential as ultrashort high-fluence X-ray sources, suitable for a wide variety of applications such as X-ray flash radiography [3], kinetic X-ray diffraction [4], and X-ray absorption spectroscopy [5].

In general, such studies would be better served by experimental diagnostic techniques which were not only spectrally resolving, but which also provided spatial discrimination of the origin of X-ray emission, and the capacity to delineate in time its spectral and spatial features. These requirements are nowhere more stringently exhibited than in the study of laser fusion plasmas where spectrally resolved data in the 0.1–50 keV range is required with micron spatial accuracy and temporal resolution in the picosecond range [6]. Such diagnostic performance would provide important information on 1) the understanding of the absorption and transport of energy in the corona of the irradiated fuel pellets, 2) the stability and hydrodynamics of the shell implosion, and 3) the character of the final fuel state. These goals have lead to the development of a wide variety of novel X-ray diagnostic instruments satisfying many of these needs. High-resolution spatial images can be provided by cylindrical [7], [8] and more complex reflective microscopes [9], by Fresnel zone plate [10] and synthetic aperture structures [11]. Time-resolved X-ray systems have been developed incorporating picosecond X-ray streak cameras [12], ultrafast X-ray framing cameras [13], and subnanosecond detectors [14]. Apart from more conventional crystal and grating dispersive elements, new spectrally discriminating soft X-ray elements have been developed in the form of multilayer structure mirrors [15] and free-standing X-ray transmission gratings [16].

In this paper, we describe the incorporation of some of this technology into instruments which provide spatially and temporally resolved detection of the X-ray emission from laser-irradiated planar and spherical targets. Broad-band spectral resolution has been incorporated with the use of either X-ray transmission gratings [17] or a large array of K-edge absorption filters [18]. Temporal resolution was provided by picosecond X-ray streak cameras. Specific technical details of each of the instruments are given, with an evaluation of their spectral, spatial, and temporal performance. Finally, discussion is made of some of the plasma parameters which these devices can diagnose, and illustrations are given from experiments performed using the single-beam 0.35 μm GDL facility on planar targets, and from studies made with the 1.05 μm 24 beam OMEGA symmetric irradiation facility at the Laboratory for Laser Energetics.

II. BROAD-BAND SPECTRALLY RESOLVING INSTRUMENTATION

Studies of transient high-density plasma phenomena ideally require X-ray diagnostic instrumentation having a broad range of spectral sensitivity, as well as high spatial and temporal resolution. Imaging systems such as pinhole cameras, X-ray

Manuscript received April 8, 1983; revised June 18. 1983. This work was supported in part by the General Electric Company, Northeast Utilities, New York State Energy Research and Development Authority, The Standard Oil Company (SOHIO), the University of Rochester, and the Empire State Electric Energy Research Corporation.

M. C. Richardson, R. S. Marjoribanks, S. A. Letzring, and J. M. Forsyth are with the Laboratory for Laser Energetics, University of Rochester, 250 East River Road, Rochester, NY 14623.

D. M. Villeneuve was with the Laboratory for Laser Energetics, University of Rochester, 250 East River Road, Rochester, NY 14623. He is now with the Division of Physics, National Research Council of Canada, Ottawa, Ont., Canada.

0018-9197/83/1200-1861$01.00

microscopes, and Fresnel zone plates provide high spatial resolution, typically a few microns, in the 0.1–10 keV range. X-ray streak and framing electrooptic cameras now provide picosecond and subnanosecond temporal resolution, respectively.

The provision of spectral resolution in these spatially and temporally resolving instruments can be accomplished in a number of ways. The most common means of attaining some measure of broad-band spectral discrimination is through the use of a set of different K-edge absorption filters. High spectral resolution and moderate spatial resolution (10's of microns) can be achieved in the soft X-ray region with focusing normal incidence grating instruments [19]. At higher X-ray energies, curved crystal spectrographs give moderate spatial resolution [20]. In addition, recent developments in X-ray multilayer fabrication offer potential for spectrally specific imaging systems [21]. X-ray streak cameras have been mated to K-edge filter [22] or multilayer mirror arrays [23] and to crystal [24] or grating [25] spectrographs to give either moderate spectral discrimination across a broad spectral range or high spectral resolution over a limited range, respectively. Until recently, there has been no instrument providing spectral resolution sufficient to discriminate between lines of highly ionized species, while at the same time possessing a broad spectral range. The instruments described in the following possess such properties.

A. Spectrally Dispersive Microscopy

Line-specific dispersed images can be produced with the incorporation of a low-dispersive-power element into the optical path of an X-ray microscope [26]. The most suitable element for this purpose is a free-standing X-ray transmission grating, which introduces negligible optical distortion, is inherently efficient, and is relatively easy to implement. Finely spaced metallic gratings having a spatial period of 300 nm (bar width 180 nm) have recently been developed with grating thicknesses of ~600 nm over areal extents of ~1 cm^2 [16]. We have integrated such a grating into the optical path of a four-channel Kirkpatrick-Baez microscope [8]. This instrument, shown in Fig. 1(a), utilizes an array of four cylindrical mirrors each of radius of curvature 32.4 m, in a fixed focus optically contacted array for greater stability. It has a total solid angle acceptance of ~10^{-6} sr, producing a 5X magnified image, 127 cm from the target with a spatial resolution of ~4 μm. The mirrors are Ni-coated, which in combination with Be and Al K-edge filters gives a spectral acceptance range of 1.5–4.5 keV under the assumption of a Boltzmann X-ray source function of temperature ~1 keV. The grating is deployed at a point along the viewing axis of the microscope, 20.3 cm from the mirror block where the four microscope image axes intersect. With a distance of 78.7 cm to the image plane, this gives a dispersion of $d\lambda/ds \approx 3.75$ Å/mm, with an effective spectral resolution in the dispersion direction of ~5 Å. The spatial resolution in the dispersion-free direction should not be significantly degraded by the imposition of the grating in the optical path. A typical image from this instrument is reproduced in Fig. 1(b), showing a multiply dispersed image of a 540 μm 1.0 μm wall glass microballoon imploded by the 1 ns 24 beam 2 kJ 1.05 μm output of the OMEGA laser facility.

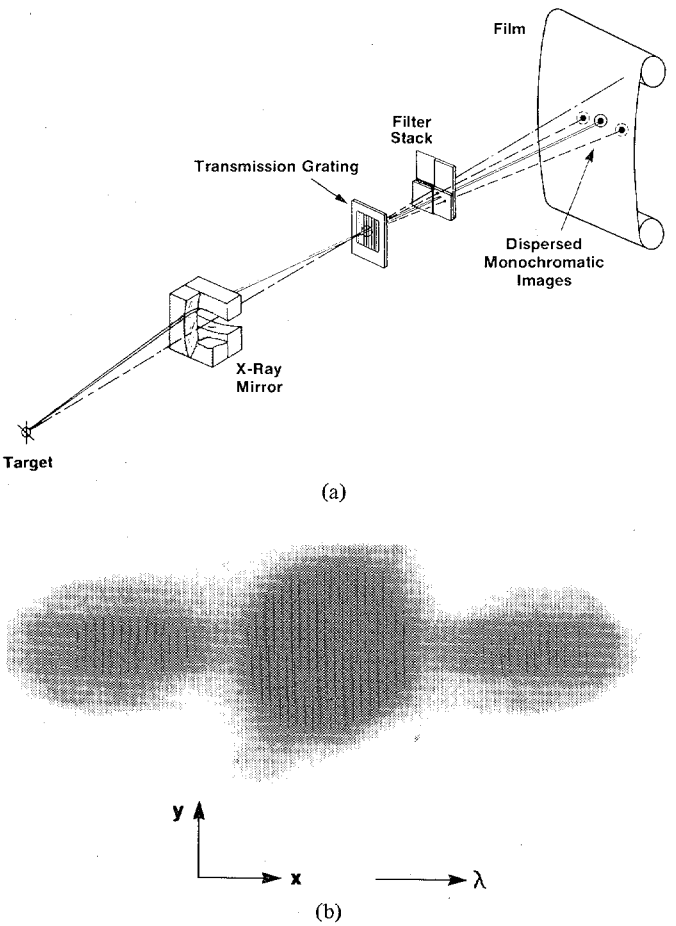

Fig. 1. (a) Kirkpatrick–Baez microscope. Provides 5X magnification with ~4 μm resolution at the source by using crossed cylindrical grazing incidence mirrors to sequentially compound line images in orthogonal directions. The four images produced may be selectively filtered in a filter stack. In the dispersive microscope, a transmission grating disperses the image spectrally in one direction. (b) Dispersed image of a 540 μm diameter glass microballoon of wall thickness 1 μm, imploded by the 24 beam symmetric irradiation from the OMEGA laser. The undiffracted (zeroth-order) X-rays form a conventional image here overexposed; first-order images are formed from different spectral components diffracted from the zeroth-order image by the transmission grating.

The central, deliberately overexposed image is one of the four (zeroth-order) undiffracted images produced by the microscope. On either side of this image can be seen the first-order dispersed images of the imploded target. Clear images of the core and corona in emission from He-like and H-like Si and Ca can be determined in the ~6 Å range. High-resolution spectrally specific images of laser fusion targets of this type will be of much value to studies of the stability of imploding shells and to the analysis of other issues associated with determining two-dimensional features of energy transport and ablation.

B. Transmission Grating Streak-Spectrograph

Transmission diffraction gratings of the type described above may be deployed in ideal low-dispersion broad-band spectrographs of high efficiency. In conjunction with an X-ray streak camera, a high time resolution (picosecond) spectrograph is created [27]. In the device constructed at LLE, shown schematically in Fig. 2(a), a transmission diffraction grating similar to the one described above [16] was mounted together with a

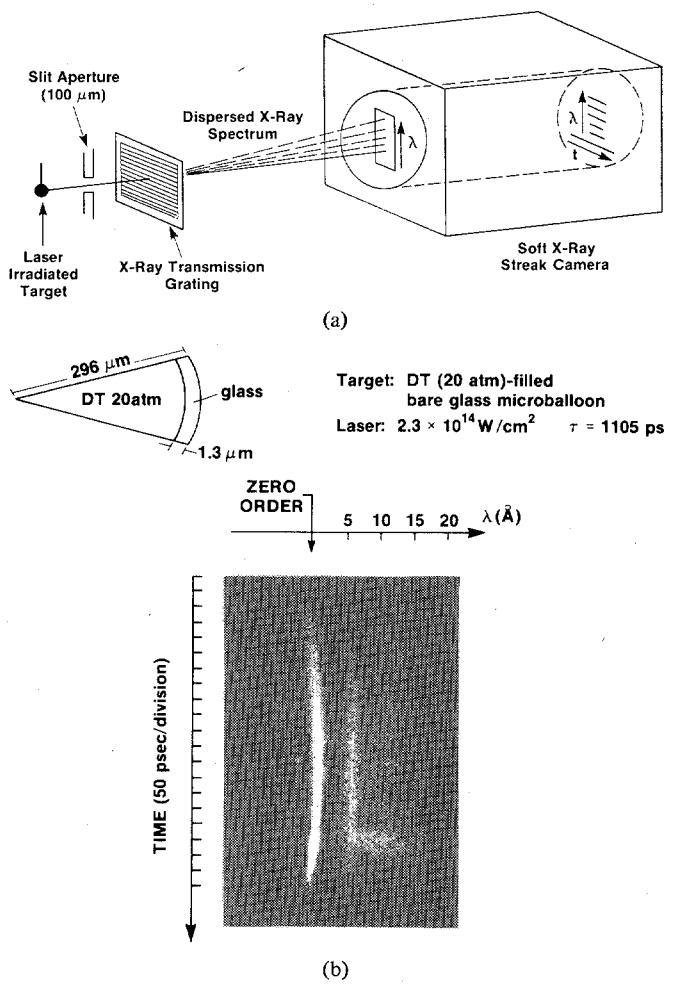

Fig. 2. (a) Transmission grating X-ray streak spectrograph. X-rays from the target pass through a slit aperture and transmission grating and are dispersed spectrally along the photocathode of the streak camera, which subsequentially disperses the spectrum in time. The film record produced represents X-ray intensity as a function of wavelength and time. (b) X-ray streak spectrograph record of a bare glass microballoon of diameter 592 μm, wall thickness 1.3 μm filled with 20 atm *DT* mixture, imploded by the OMEGA laser system (intensity ~ 2.3 × 10^{14} W · cm^{-2}, pulse length ~1105 ps). Wavelength in angstroms and time (50 ps/div) form orthogonal axes. The undiffracted component, or zeroth-order component (marking the position from which wavelength is proportional to distance dispersed) lasts throughout the laser pulse. The prominent emission at about 6 Å is Si emission from target shell material; at relatively late times, a broad spectral feature marks the peak implosion of the target.

150 μm slit aperture in the path between the target and the streak camera. The X-ray emission from the laser-irradiated target is dispersed along the admittance slit of the streak camera which subsequently disperses the spectrum in time.

The streak camera [28] employed a photocathode which consisted of 10 nm of gold evaporated onto a 1.5 μm thick stretched polypropylene substrate. The polyimide substrate of the transmission grating blocked most X-rays less energetic than 500 eV; the efficiency of the grating in diffracting X-rays more energetic than 500 eV was about 0.1. X-rays that passed undiffracted formed the zeroth order, from which position the distance of dispersion along the photocathode was proportional to wavelength. The ability of the device to resolve higher energy X-rays, only slightly dispersed in the first order, from the zeroth-order diffraction imposed an upper energy of ~10 keV on the dispersed spectrum.

The spectral resolution and dispersion can be determined with reference to Fig. 3, which shows the geometrical arrangement of the target, transmission grating–slit combination, and streak camera. For the present work, the distance from target to grating (L) was 108 cm, and from the grating to the streak camera photocathode D = 110 cm. The slit width A was 150 μm, and the grid spacing was d = 0.3 μm. Thus, the spectral resolution, defined by the equation [27]

$$\delta\lambda = \left(\frac{(S+A)}{L} + \frac{A}{D}\right)d$$

gives, for a target source size, $S \sim 400$ μm, characteristic of the initial diameter of spherical targets in our experiments, a value of $\Delta\lambda \sim 1.9$ Å. The resolution is explicitly dependent on the extent of the emitting region; for sources smaller than about twice the slit aperture size, the resolution approaches a limiting value of ~0.8 Å. The spectral dispersion, derived from the Bragg condition, $\sin\theta = m\lambda/d$, is

$$d\lambda/d\theta = d\cos\theta/m$$

where m is the order number, giving a dispersion in the streak camera cathode plane of $d\lambda/ds \approx d/mD = 2.73$ Å/mm^{-1}. Thus, the 1 cm long photocathode would include all of the spectrum above the carbon K-edge passed by the polyimide substrate of the transmission grating. The assumption of a streak camera spatial resolution of 10 *lp* mm^{-1} at the photocathode would then imply ~3 spatial resolution elements per spectral resolution element for the minimum source size. The temporal resolution of the streak camera was estimated to be ~30 ps.

The large spectral range and good temporal resolution of this device afforded by the high efficiency of the grating compensate for the relatively low spectral resolution, and make the device particularly suitable for qualitative and comparative studies. This is illustrated in Fig. 2(b), which shows the time-resolved spectrum of the X-rays emitted from a glass microballoon [29], of 594 μm diameter and wall thickness 1.3 μm filled with 20 atm of *DT*. This was uniformly irradiated with a 1 ns pulse from the 24 beam OMEGA laser system, with a total energy of 2.8 kJ. The brightest time-smeared signal in Fig. 2(b) is that of the zeroth-order undispersed X-ray emission. However, emission in the first order at ~6 Å, corresponding predominantly to emission from Si in the glass shell, can be seen to persist throughout the irradiation of the target. At stagnation of the implosion, the core temperature increases, giving rise to brief bright emission of other line radiation, and X-ray continuum in the 1–20 Å range.

C. X-Ray Filter Streak Spectrometer

The performance of the streak transmission grating spectrograph can be compared to a second time-resolving spectrometer which utilizes an X-ray streak camera in conjunction with an array of 14 X-ray K-edge filters [Fig. 4(a)]. A streak spectrograph of this type provides time-resolved spectral information in restricted regions of the spectrum, determined by the convolution of the source spectral distribution, the K-

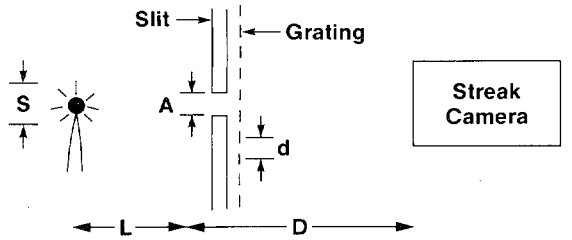

Fig. 3. Schematic of transmission grating streak camera system.

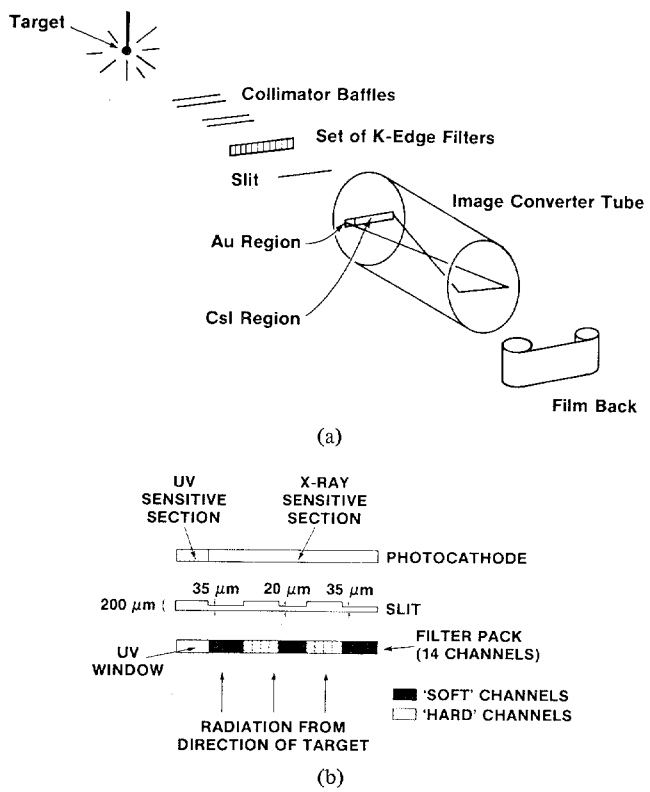

Fig. 4. (a) X-ray filter streak spectrometer. Uses a set of *K*-edge filters arranged at the photocathode of an X-ray streak camera. A set of collimator baffles and permanent magnets comprise a plasma divertor in this reentrant design. The photocathode included two regions, one with a solid CsI cathode in a Be foil for sensitive X-ray detection, and another of Au deposited on stretched polypropylene located behind a quartz window, used to record a fiducial of the laser pulse. (b) Spectrometer filter pack. Grouped "soft" and "hard" channels separately, using various width "streak slits" to tailor the overall flux in the groups of channels. This normalization of filter groups improved the useful dynamic range of the device.

edge filter transmission, and the photocathode response function. The use of a number of filtered channels then permits the determination of the overall spectrum across a broad spectral range. This device [30], [18] utilizes a 100 nm solid CsI photocathode [31] deposited on a 25 μm thick Be substrate. In addition to the latter, a separate photocathode region, consisting of 10 nm of gold evaporated onto a 25 μm polyethylene substrate, provided a degree of sensitivity to 0.35 μm laser light used in certain experiments described below [32]. This second photocathode lay behind a fused silica window, which passed ultraviolet light while blocking X-rays.

The continuum spectrum emitted from laser-produced plasmas characteristically produces highest X-ray fluences at lower X-ray energies. For this reason, a streak slit of varied width is used to tailor the flux onto the photocathode [Fig. 4(b)]. With the signal in each channel approximately balanced in the camera output, inherent nonlinearities in the streak camera itself would have less impact on inferences of relative intensity between channels, and the effective spectral dynamic range is improved.

The device records on film X-ray intensity as a function of time, for each of a number of slightly differing spectral windows determined by the filters used. Typical data are shown in Fig. 5. This shows the spectrum emitted by an imploding glass microballoon, of diameter 400 μm and wall thickness 1 μm, filled with 20 atm *DT* and 2 atm Ar, irradiated with 2 kJ, 1 ns, 1.05 μm radiation from the OMEGA system. Thirteen separate filter channels recorded the X-ray emission, from which the temporal evolution of the X-rays in specific spectral bands could be determined.

As an aid in the reduction of data, a novel technique has been developed in which film characteristics are automatically deconvolved in the normal operation of a slightly modified differentially driven comparing densitometer, without the use of digital reduction [33]. In this scheme, the reference density wedge of the densitometer is replaced by a replica of itself made by contact printing it onto a strip of the same film used for recording the data being densitometered. The replica film wedge is produced using a light source which sensitometrically simulates the characteristics of the phosphor output of the streak camera intensifier. This replica is developed under conditions identical to those used for the streak camera data. In use, the comparative densitometer will seek a density on the film reference wedge which matches that of the data being reduced, and will record the position along that wedge as the densitometer output. Since the film reference wedge was produced from a linear optical density wedge, this position is then proportional to the logarithm of the exposure that produced that film's optical density. As the reference wedge film has identical characteristics to the data film being reduced, the densitometer provides an output which is proportional to the logarithm of the initial exposure. The effectiveness of this method is demonstrated by densitometering a film density wedge agains a similar film wedge used as a reference wedge (Fig. 6). The film characteristics are removed and a linear trace of slope 1 results, showing that the use of the nonlinear density wedge produces a simple densitometer signal proportional to the logarithm of the original exposure. This approach, as can be seen from Fig. 6, is also particularly effective in unfolding the toe of the film response curve.

III. Laser-Produced-Plasma Diagnostics

A. Temperature History

The usefulness of the devices described above can be demonstrated by illustrating specific plasma parameters which they are effective in diagnosing. The X-ray filter streak spectrometer described above has been used to determine the temporal development of the temperature of a plasma produced by the irradiation of planar CH targets with single beam 450 ps pulses of 0.35 μm laser light [32]. In these experiments, the planar targets were oriented so as to direct the specularly reflected light onto the UV-sensitive section of the streak camera photo-

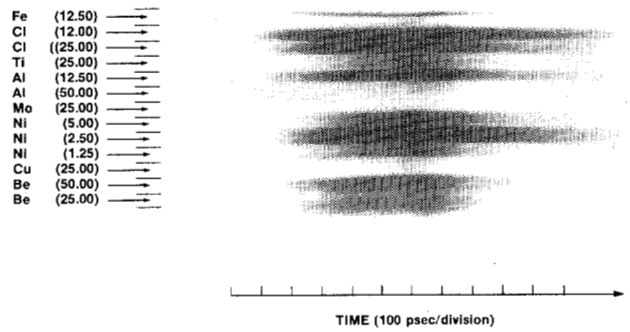

Fig. 5. X-ray filter streak spectrometer record shows emission from imploding glass microballoon 400 μm in diameter filled with 20 atm *DT* and 2 atm Ar. Target wall thickness was 1 μm, with laser intensity $\sim 3 \times 10^{14}$ W · cm^{-2}. Filter materials and thicknesses are annotated at the left; the lower axis marks time from left to right.

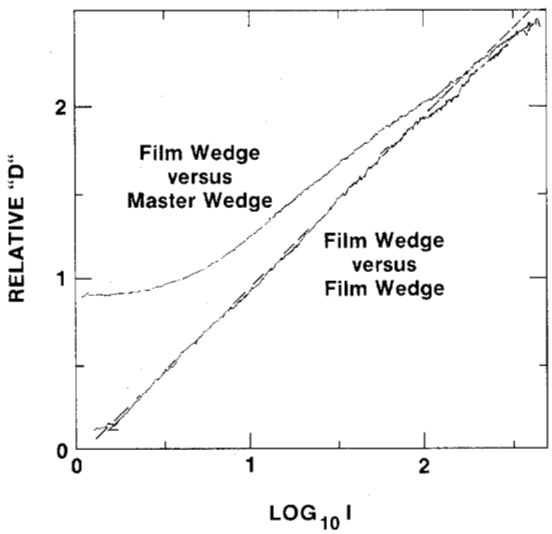

Fig. 6. Film wedge densitometer. A film strip produced by contact printing through a linear density wedge is densitometered conventionally, and with the method outlined. Conventionally densitometered in reference to a glass linear density wedge (upper curve), the trace shows the nonlinear film characteristics, and density rising from the fog level.

cathode. This sample of the scattered light provided a real streak-time fiducial of the irradiating pulse, with reference to which the delay and shape of the X-ray emission pulse could be established. The streak camera was situated at 22° to the other side of target normal, viewing the radiating plasma and collecting specularly scattered laser light. In Fig. 7, reduced data from such a shot are reproduced, showing the signals in a number of different streak channels and their delay relative to the laser peak intensity fiducial. Also shown is a prediction of the output of one of these channels drawn from a one-dimensional hydrocode (LILAC) simulation of the experiment. Such comparisons are useful in that they can help support assumptions of absorption and energy transport mechanisms made in the hydrodynamic code.

With the assumption of a single-Maxwellian X-ray continuum distribution, the predicted spectra for a number of temperatures were convolved with the filter spectral transmission functions and photocathode spectral response. Ratios of intensities for different channels of the observed data were then compared to predicted values to arrive at an estimate of

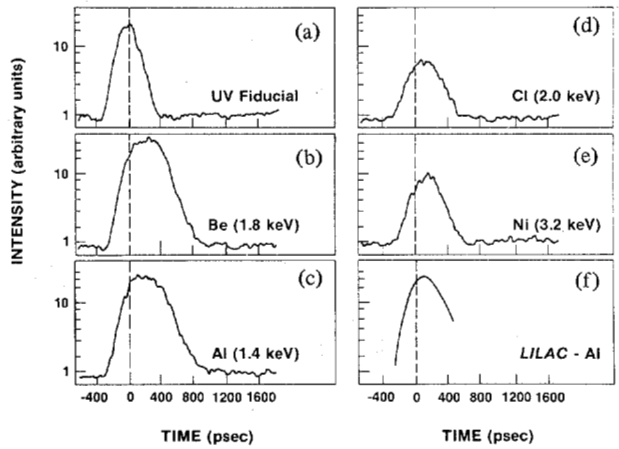

Fig. 7. X-ray filter streak spectrometer reduced data from UV laser-irradiated planar plastic target. For *K*-edge filter channels [their approximate *K*-edge spectral responses are indicated are in (b)–(e)], the intensity scale is relative only, and has not been normalized for each channel separately. (a) shows the fiducial signal produced by 0.35 μm laser light scattered specularly from the target into a UV sensitive section of the photocathode. (f) shows, for comparison, the output of the Al channel as predicted by the one-dimensional hydrocode LILAC; general shape and delay of peak relative to the laser are reproduced.

the temperature at several times during the plasma emission. For these particular conditions, it was found that the plasma temperature was essentially constant (Fig. 8), during and shortly after the irradiating laser pulse.

B. Energy Transport

Central to the success of many applications of laser-produced plasmas, particularly laser fusion, is an accurate understanding of the transport of absorbed laser energy from the critical density region into the cold solid material. This subject has undergone considerable experimental investigation in the past few years, particularly with planar targets. In general, these studies have tended to support a model in which thermal energy transport into the target is strongly inhibited. Spectroscopic diagnosis of X-ray emission from specially constructed targets is a common diagnostic in these studies [34], [35]. In this approach, the analysis of the intensities of characteristic X-ray lines from layers of particular materials situated at various depths in low Z targets leads to an effective measurement of the progress of the heat front into the target. With the availability of uniform irradiation facilities, these studies can now be made in spherical geometry, more closely approximating a one-dimensional experimental situation which can be more easily modelled theoretically [36], [37]. Time-resolved X-ray spectroscopic diagnosis in such experiments gives the possibility of following the progress of the ablation front in time, and potentially of delineating its actual form.

Preliminary studies toward this end have been made with the devices described above. The multi *K*-edge filter streak spectrometer was used to examine thermal transport in solid spherical targets of low Z (CH), at intensities in the range of $1\text{-}4 \times 10^{14}$ W · cm^{-2}. Specially constructed targets, consisting of 400 μm diameter solid spheres overcoated with a thick layer of Al, a variable thickness of parylene (CH), and a very thin (0.03 μm) layer of KCl were used. Uniform nanosecond

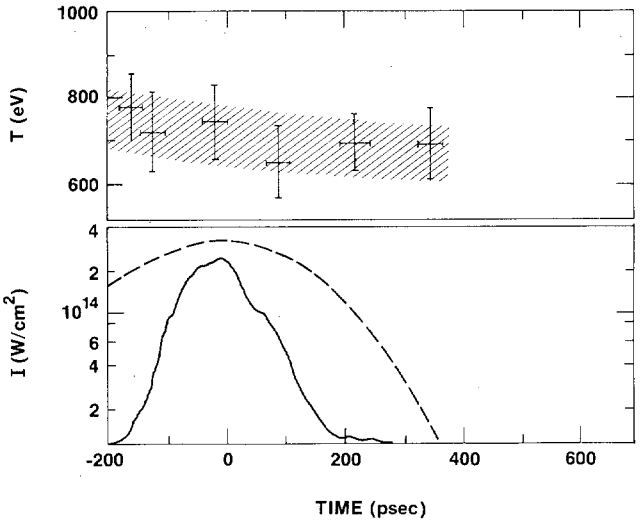

Fig. 8. The temperature deduced from thermal X-ray continuum fitting to channel intensity ratios is essentially independent of time during the laser pulse (top). The laser pulse (lower figure, dotted line) is reconstructed about the UV fiducial pulse on the assumption that the photocathode response, presumed nonlinear at 350 nm, preserves the peak of the scattered pulse and that the peak of the scattered pulse corresponds to the peak of the incident laser pulse.

1.05 μm irradiation of these targets was provided by 24 beams of OMEGA. Fig. 9 shows some typical results drawn from shots on targets having layers of CH of thickness 2, 4, and 6 μm. The thin KCl layer was added to provide a relative time fiducial to the spectrometer signals. The figure shows the intensity in one of the *K*-edge spectral channels as a function of time, utilizing the film reduction routine referred to in the previous section. Following the initial onset of X-ray emission from the KCl, the signal remains almost constant while the ablation front propagates through the CH layer. The steep rise in the signal indicates the propagation of energy to the Al layers, and thereby gives an indication of the speed with which the CH layer was ablated. From these studies, the time dependence of the burnthrough in the CH can be determined for specific irradiation conditions [Fig. 9(b)]. This indicates that throughout the Gaussian laser pulse, the rate at which material is ablated is approximately constant. At an incident laser intensity of $\sim 4 \times 10^{14}$ W $\cdot$ cm^{-2}, this measurement would indicate a mass ablation rate of 4.7×10^{5} g $\cdot$ cm^{-2} $\cdot$ s^{-1}. Future studies will concentrate on analyzing in more detail the shape and progress of the heat front relative to the incident intensity profile.

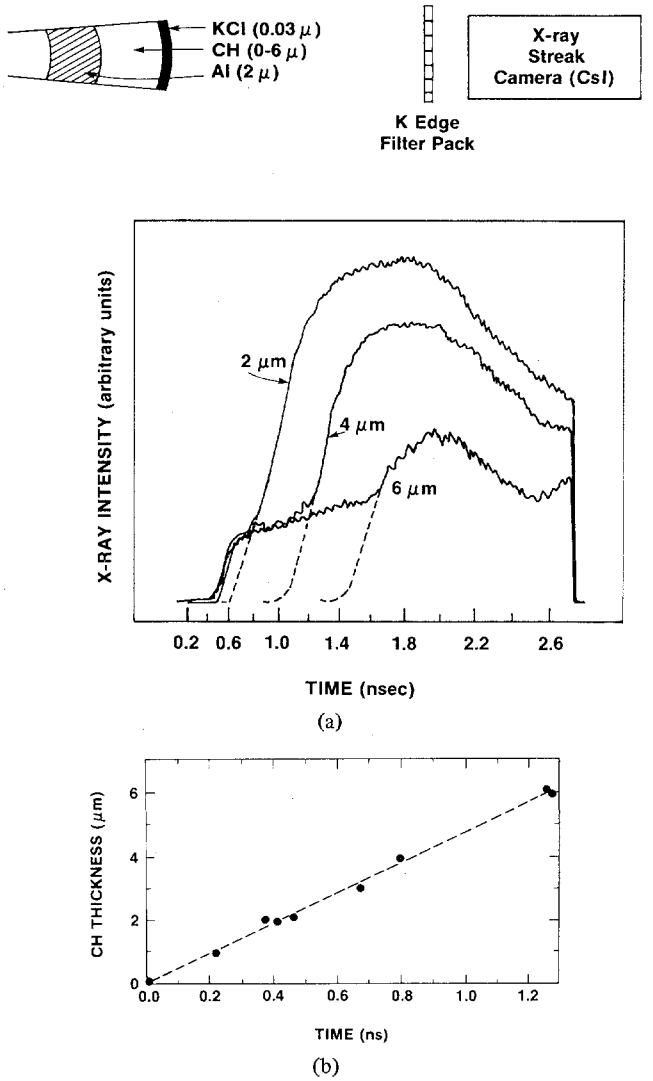

Fig. 9. Time-resolved burnthrough measurements of energy transport. (a) X-ray filter streak spectrometer traces of the emission from coated Al microspheres show that the time of onset of emission from the Al is delayed uniformly by the addition of CH overcoat. Results for plastic thicknesses of 2, 4, 6 μm show delay in burnthrough, as measured from the onset of emission from the thin KCl "marker" layer, increases with plastic thickness. (b) The relation between plastic thickness and time of burnthrough, determined from data similar to that of Fig. 8(a), shows the rate of burnthrough to be fairly constant throughout the laser pulse.

C. Core Emission Spectroscopy

In the study of imploding *DT*-filled microspheres, the final conditions of the core are often inferred from conditions of the stagnating target shell since the low-*Z* fill gases result in little diagnosable radiation. To derive a signature of the core conditions directly, some authors [38], [39] have included in the fill gas a small mixture of a higher-*Z* gas, typically Ne or Ar, the emission from which has been examined using time-integrated spectroscopy. Similar targets have now been studied with the present time-resolving spectrometers. In these particular experiments, the targets were high aspect ratio microspheres filled with 20 atm of *D*–*T* mixture plus, typically, 2 atm of Ar, and were irradiated uniformly by nanosecond pulses at $\sim 4 \times 10^{14}$ W $\cdot$ cm^{-2} from the OMEGA system.

Fig. 10 shows the transmission grating streak spectrograph record of a *DT* + Ar filled glass microscope of diameter 414 μm and wall thickness of 0.84 μm uniformly driven at 3.8×10^{14} W $\cdot$ cm^{-2}. The raw data show the zeroth-order (undiffracted) component at the left, and various spectral features with various durations streaked at positions displaced proportional to wavelength. In particular, there is a spectrally broad feature localized along the time axis, which can be attributed to the peak of compression of the target shell. Accompanying the raw data is a series of densitometer traces made across the spectrum at different streak times as indicated. At early times, the prominent features are the zeroth-order component, and a peak due to *K*-shell Si emission from the target shell. At later

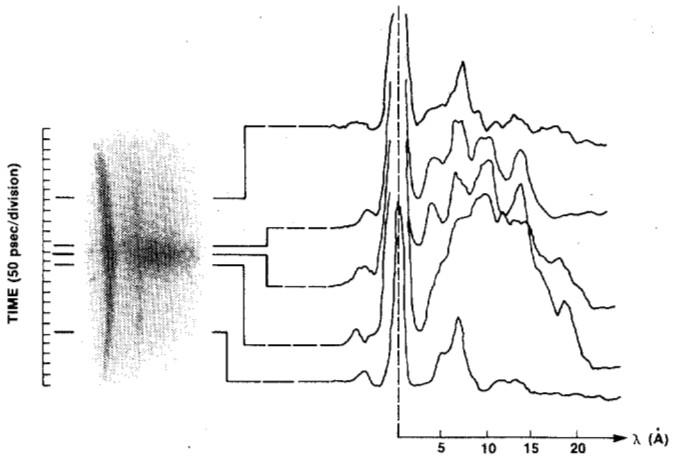

Fig. 10. Core emission spectroscopy. This transmission grating streak spectrograph record shows emission from a DT + Ar filled (20 atm + 2 atm, respectively) glass microballoon (diameter 414 μm, wall thickness 0.84 μm) uniformly driven at 3.8×10^{14} W · cm^{-2}. Raw data are shown at left; at the right are densitometer traces providing spectra at a number of times in the streak. In addition, the zeroth-order component, spectral features attributable to target components [Si, O, Na, and the continuum implosion feature noted in Fig. (6)], there is emission due to Ar, at about 4 Å, early in the peak of compression.

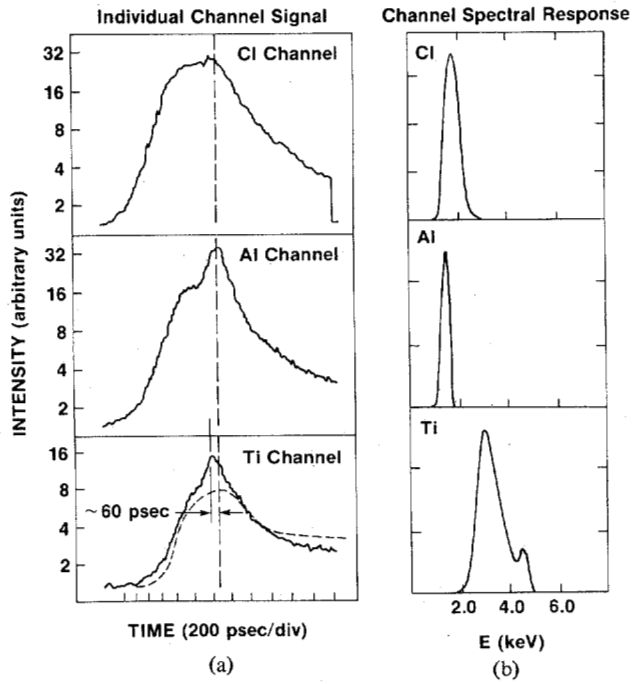

Fig. 11. Core emission spectroscopy. Reduced data from the X-ray filter streak spectrometer show qualitative differences in the signals of several channels. The Cl channel signal rises roughly as the laser intensity and decays; the Al channel signal is similar, but with an additional peak superimpsed, which is attributed to a larger relative contribution of emission from target materials (particularly Si) at stagnation of the implosion. The Ti channel shows a sharp peak attributed to Ar emission from the core at peak compression. This feature is not present in the absence of Ar filled (dotted line).

times, but early in the emission from the compressed core, a number of other spectral features arise which are attributed to shell constituents (Si, Na, O). In addition, there is also a peak arising at a wavelength consistent with Ar. There may be an involvement of Ca in the target, but the feature dissipates later in the emission from the compression core before the emission from identifiable target components subsides. At late times, the Si emission predominates.

The X-ray filter spectrometer provides data which augment these results. The spectral content of the filter channels is better identified when this device is used in conjunction with the transmission grating streak spectrograph. In the record from this same shot (Fig. 5), the filter device shows emission which peaks in all channels at the same time, except for the Ti and Ni channels, for which it is apparent the emission is earlier and qualitatively different. Comparing channel spectral responses for several of the filters used (Fig. 11), it would be expected that emission from the K-shell of Si would be more heavily weighted by the narrow Al foil channel than by the shifted and broader Cl channel. Whereas the Cl channel has a form which rises and falls on the same time scale as the laser, the Al channel has an additional peak superimposed on a similar form. This structure is attributed to K-shell emission from Si in the stagnating glass shell. The Ti channel has a distinctly shifted spectral response, admitting the Ar K-shell emission but largely excluding emission from Si. The result is a qualitatively different trace exhibiting a peak ~60 ps in advance of that in the adjacent Al channel. Additionally, in the absence of Ar seed gas in the fill gas, this signal is changed to the rounded shape shown by the dotted line in Fig. 10. Thus, the emission from Ar in the core itself is determined to be ~60 ps in advance of the emission from the stagnating shell, possibly suggestive of a converging shock transmitted through the core and rebounding against the target shell.

The extent of the region from which the Ar emission originated in the case of these target implosions was diagnosed with

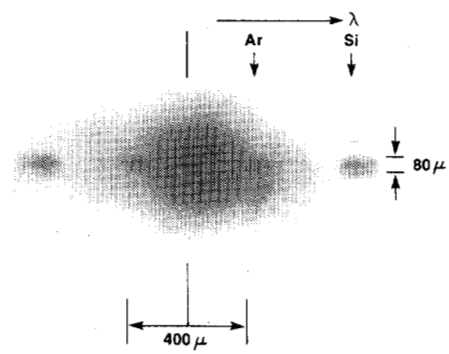

Fig. 12. Dispersive X-ray micrograph of a 400 μm diameter, 1 μm wall, glass microballoon filled with 20 atm DT and 2 atm Ar, irradiated with 2 kJ, in 1 ns from the 24 beam OMEGA system. Although the central zeroth-order image is deliberately overexposed, clear images, in first order, composed of the k-shell emission of Ar and Si from the compressed core are evident.

the aid of the dispersive microscope. The relevant image (Fig. 12) gives a clear identification of the extent of the K-shell Ar and Si emission from the compressed core in the first-order diffracted images on either side of the central undiffracted image. As can be seen, the spatial extent of the Ar emission is ~40 μm, whereas the Si emission originating from the compressed stagnated shell originates from a somewhat larger region (~80 μm). With knowledge of the spatial character of the Ar line emission, the width of the L_β lines gives a indication of peak Ar density [39], which leads to an estimate of the core density-radius product for Ar, $\rho R \sim 2.5 \times 10^{-3}$ g · cm^{-2} in close agreement with predicted values [40].

IV. Summary

This paper summarizes some recent progress made in the application of broad spectral band time and space-resolved X-ray diagnostics to the understanding of processes occurring in laser-produced plasmas. The future development of laser fusion and other applications of laser-produced plasmas rests heavily on the comprehensive diagnosis of many complex features of the interactions. This will be greatly facilitated by the development of X-ray diagnostic techniques possessing high spatial and temporal resolution, with spectral sensitivity optimized to the issues of interest.

Acknowledgment

Part of this work, that involving the use of free-standing X-ray transmission gratings, would not have been possible without the inspiration and advice of N. M. Ceglio, who originally perceived this approach to X-ray spectroscopy, and A. M. Hawryluk, who perfected the development of submicron transmission X-ray structures. The technical support of T. Chin, G. Gregory, and W. Watson is also appreciated.

References

[1] J. H. Nuckolls, L. Wood, A. Thiessen, and G. Zimmerman, "Laser compression of matter to super high densities–thermonuclear (CTR) applications," *Nature*, vol. 239, pp. 139–142, 1972.

[2] R. W. Waynant and R. C. Elton, "Review of short wavelength laser research," *Proc. IEEE*, vol. 64, p. 1059, 1976.

[3] M. H. Key, P. T. Rumsby, R. G. Evans, C.L.S. Lewis, J. M. Ward, and R. L. Cooke, "Study of ablatively imploded spherical shells," *Phys. Rev. Lett.*, vol. 45, p. 1801, 1980.

[4] R. D. Frankel and J. M. Forsyth, "Nanosecond X-ray diffraction from biological samples with a laser-produced plasma source," *Science*, vol. 204, pp. 622–624, 1979.

[5] P. J. Mallozzi, R. E. Schwerzel, H. M. Epstein, and B. E. Campbell, "Laser EXAFS. Fast extended X-ray absorption fine structure spectroscopy with a single pulse of laser produced X-rays," *Science*, vol. 206, p. 353, 1979; also, B. Yaakobi, H. Deckman, P. Bourke, S. Letzring, and J. M. Soures, "X-ray absorption fine structure measurement using a laser compressed target as a source," *Appl. Phys. Lett.*, vol. 37, p. 767, 1980.

[6] D. T. Attwood, "Diagnostics for laser fusion–Plasma physics on the scale of microns and picoseconds," *IEEE J. Quantum Electron.*, vol. QE-14, p. 909, 1978.

[7] P. Kirkpatrick and A. V. Baez, "Formation of optical images with X-rays," *J. Opt. Soc. Amer.*, vol. 38, p. 766, 1948.

[8] F. D. Seward and T. M. Palmier, "A simple X-ray microscope for photographing laser produced plasmas," *Rev. Sci. Instrum.*, vol. 46, p. 204, 1975.

[9] R. H. Price, "X-ray microscopy using grazing incidence reflection optics," in *Proc. APS Topical Conf. on Low Energy X-ray Diagnostics*, D. T. Attwood and R. L. Henke, Eds., AIP Conf. Proc. No. 75, 1981, p. 189.

[10] G. Schmahl, D. Rudolph, B. Niemann, and O. Christ, "X-ray microscopy of biological specimens with a zone plate microscope," in *Ann. N.Y. Acad. Sci.*, vol. 342, p. 368, 1980.

[11] N. M. Ceglio, D. T. Attwood, and E. V. George, "Zone plate coded imaging of laser produced plasmas," *J. Appl. Phys.*, vol. 48, p. 1566, 1977.

[12] P. R. Bird, D. J. Bradley, A. G. Roddie, W. Sibbett, M. H. Key, M. Lamb, and C.L.S. Lewis, "Picosecond chromagraphy of X-ray wavelengths," in *Proc. 11th Int. Conf. High Speed Photography*, 1974, p. 118; also, L. W. Coleman and C. F. McConaghy, "Ultrafast X-ray streak camera," in *Proc. 11th Int. Conf. High Speed Photography*, 1974, p. 196; and, Yu. S. Kasyanov, A. A. Malyutin, M. C. Richardson, and V. K. Cherokin, "Picosecond X-ray streak camera studies," in *Proc. 11th Int. Conf. High Speed Photography*, 1974, p. 561.

[13] G. Eschard, "The microchannel plate: A survey of the possibilities of channel multiplier arrays in nanosecond and picosecond detection and imaging," in *Proc. 11th Int. Conf. High Speed Photography*, 1974, p. 163.

[14] H. N. Kornblum and V. W. Slivinsky, "Flat response subkiloelectrivolt X-ray detection with a subnanosecond response," *Rev. Sci. Instrum.*, vol. 49, p. 1204, 1978.

[15] E. Spiller, "Evaporated multilayer dispersive elements for soft X-rays," in *Proc. Topical Conf. Low Energy X-ray Diagnostics*, D. T. Attwood and R. L. Henke, Eds., AIP Conf. Proc. no. 75, 1981, p. 124; also, T. W. Barbee, "Sputtered, layered synthetic microstructure (LSM) dispersion elements," in *Proc. Topical Conf. Low Energy X-ray Diagnostics*, D. T. Attwood and R. L. Henke, Eds., AIP Conf. Proc. no. 75, 1981, p. 131.

[16] A. M. Hawryluk, N. M. Ceglio, R. H. Price, J. Melngaillis, and H. I. Smith, "Soft X-ray spectroscopy using thick gold transmission gratings of 0.2 to 0.3 μm spatial periods," in *Proc. Topical Conf. Low Energy X-ray Diagnostics*, D. T. Attwood and R. L. Henke, Eds., AIP Conf. Proc. no. 75, 1981, p. 286.

[17] S. A. Letzring, R. S. Marjoribanks, M. C. Richardson, and D. M. Villeneuve, "Time-resolved X-ray spectroscopy of symmetrically imploded targets," in *Proc. 15th Int. Cong. High Speed Photography, S.P.I.E.*, vol. 348, 1982, p. 325.

[18] R. S. Marjoribanks, S. A. Letzring, and M. C. Richardson, "Time-resolved X-ray spectroscopy for laser fusion studies," in *Proc. 15th Int. Cong. High Speed Photography, S.P.I.E.*, vol. 348, 1982, p. 318.

[19] U. Feldman, G. A. Doschek, D. K. Prinz, and D. I. Nagel, "Space-resolved spectra of laser-produced plasmas in the XUV," *J. Appl. Phys.*, vol. 47, pp. 1341–1350, 1976.

[20] L. M. Belyaev, A. R. Gil'varg, Yu. A. Mikhailov, S. A. Pikenz, G. V. Skilzkov, A. Ya. Faenov, and S. I. Fedotov, "Recording of X-ray spectra with one- and two-dimensional spatial resolution by means of a spherical crystal analyzer," *Instrum. Exp. Tech.* (USSR), vol. 20, p. 855, 1977.

[21] J. H. Underwood and T. W. Barbee, "Soft X-ray imaging with a normal incidence mirror," *Nature*, vol. 294, p. 429, 1981.

[22] P.H.Y. Lee and M. D. Rosen, "Time-resolved high-energy X-ray spectra of laser-irradiated targets," *Phys. Rev. Lett.*, vol. 42, p. 236, 1979.

[23] G. L. Stradling, D. T. Attwood, and R. L. Kauffman, "A soft X-ray streak camera," *IEEE J. Quantum Electron.*, vol. QE-19, pp. 604–615, Apr. 1983.

[24] M. H. Key, C.L.S. Lewis, J. G. Lunney, A. Moore, J. M. Ward, and R. J. Tearega, "Time-resolved X-ray spectroscopy of laser produced plasmas," *Phys. Rev. Lett.*, vol. 44, p. 1667, 1980.

[25] M. H. Key, M. J. Lamb, D. Landhaer, C.L.S. Lewis, J. A. Lunney, and R. K. Thareja, "Applications of streak camera techniques to temporal spatial and spectral resolution of VUV and X-ray emission from laser produced plasmas," 10th Europ. Conf. Laser Interaction, 1976, unpublished.

[26] N. M. Ceglio, A. M. Hawryluk, and H. Price, "Imaging X-ray spectrometer for laser fusion application," *Appl. Opt.*, vol. 21, p. 3955, 1982.

[27] N. M. Ceglio, R. L. Kauffman, A. M. Hawryluk, and H. Medecki, "A time-resolved X-ray transmission grating spectrometer for investigation of laser produced plasmas," Lawrence Livermore National Laboratory Report UCRL-81800, unpublished, 1982.

[28] S. A. Letzring, E. I. Thorsos, W. D. Friedman, W. Seka, and J. E. Rizzo, "An absolutely timed X-ray streak camera for laser fusion experiments," *Rev. Sci. Instrum.*, to be published.

[29] Large aspect ratio spherical glass microballoons utilized in the study were fabricated by KMS Fusion Inc., and characterized and assembled at LLE by B. P. Oil Inc., a subsidiary of Standard Oil of Ohio (SOHIO).

[30] P. A. Jaanimagi and M. C. Richardson, "Streak camera for picosecond X-ray diagnostics," *Rev. Sci. Instrum.*, vol. 54, p. 1095, 1983.

[31] J. E. Bateman and R. J. Apsimon, "A new photocathode for X-ray imaging intensifiers operating in the 1–50 keV region," in *Proc. 7th Symp. Photo-Electronic Image Devices*, 1981, B. L. Morgan and D. L. McMullan, Eds; also, "Relative responses of CsI and Au photocathodes to 70 ps, 500 eV X-ray pulses," *Appl. Phys. Lett.*, vol. 37, p. 782, 1980.

[32] R. S. Marjoribanks, M. C. Richardson, J. Delettrez, S. A. Letzring, W. Seka, and D. M. Villeneuve, "Time-resolved X-ray spectrometry of UV laser produced plasmas," *Opt. Commun.*, vol. 44, pp. 113–116, 1982.

[33] R. S. Marjoribanks, unpublished.

[34] W. Seka, J.-L. Schwob, and C. Breton, "Multilayer targets as a diagnostic tool for laser-produced plasmas," *J. Appl. Phys.*, vol. 42, p. 315, 1971.
[35] B. Yaakobi and T. C. Bristow, "Measurement of reduced thermal conduction in (layered) laser-target experiments," *Phys. Rev. Lett.*, vol. 38, p. 350, 1977.
[36] T. J. Goldsack, J. D. Kilkenny, B. J. MacGowan, P. F. Cunningham, C.L.S. Lewis, M. H. Key, and P. T. Rumsby, "Evidence for large heat fluxes from the mass ablation rate of laser irradiated spherical targets," *Phys. Fluids*, vol. 25, pp. 1634–1643, 1982.
[37] B. Yaakobi, J. Delettrez, R. L. McCrory, R. Marjoribanks, M. C. Richardson, D. Shvarts, J. M. Soures, C. Verdon, D. M. Villeneuve, T. Boehly, R. Hutchison, and S. Letzring, "Thermal transport measurements in 1.05 μm laser irradiation of spherical targets," in *Laser Interaction and Related Plasma Phenomena*, vol. 6. New York: Plenum, 1982.
[38] B. Yaakobi, S. Skupsky, R. L. McCrory, C. F. Hooper, H. Deckman, P. Bourke, and J. M. Soures, "X-ray spectroscopy of laser imploded targets," *Phil. Trans. Roy. Soc. London*, vol. A300, pp. 623–630, 1981.
[39] B. Yaakobi, D. M. Villeneuve, M. C. Richardson, J. M. Soures, R. Hutchinson, and S. A. Letzring, "X-ray spectroscopy measurements of laser compressed Ar-filled shells," *Opt. Commun.*, vol. 43, p. 343, 1982.
[40] M. C. Richardson *et al.*, "Direct drive laser fusion experiments with the OMEGA laser system," in *Plasma Physics and Controlled Nuclear Fusion Research 1982*, vol. 1. Vienna: IAEA, 1982, p. 477.

Martin C. Richardson (M'72–SM'81) received the Ph.D. degree from the University of London for work performed in the areas of high-power lasers, nonlinear optics, and laser–plasma interactions carried out at the Culham Laboratory, UKAEA.

In 1967 he joined the National Research Council of Canada where he was involved in research programs on high-power UV preionized gas laser technology, picosecond pulse development, ultrafast streak camera development, multiphoton molecular dissociation, and laser-produced plasma. Since 1975 his interests have centered on fusion with both CO_2 and ND:glass lasers. Since 1980 he has been at the University of Rochester Laboratory for Laser Energetics where he is currently Group Leader responsible for experiments on the 24 beam OMEGA laser facility.

Dr. Richardson is an Associate Editor of the IEEE JOURNAL OF QUANTUM ELECTRONICS. He is a member of the American Physical Society and the Optical Society of America.

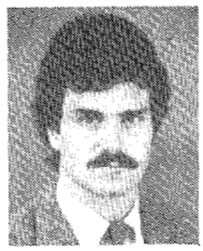

Robin S. Marjoribanks was born in Toronto, Ont., Canada, on August 9, 1956. He received the B.Sc. degree in mathematics and physics from the University of Toronto in 1978, the M.Sc. degree in physics from the University of Toronto in 1981, with thesis research in laser–plasma physics, conducted under Dr. M. C. Richardson at the National Research Council of Canada, and the M.S. degree in engineering at the University of Rochester, Rochester, NY, where he is currently pursuing the Ph.D. degree in plasma physics as a Fellow of the University's Laboratory for Laser Energetics, with the support of the Natural Sciences and Engineering Research Council of Canada.

His current research interests include the use of time-resolved X-ray spectroscopy in studies of energy transport and atomic physics of laser-driven plasmas.

S. A. Letzring, photograph and biography not available at the time of publication.

James M. Forsyth was born in Niagara Falls, NY on April 21, 1942. He received the B.S. and Ph.D. degrees in optics from the University of Rochester, Rochester, NY, completing his thesis work in 1968.

He served on the faculty of the Institute of Optics, University of Rochester, until 1979 when he became a Senior Scientist in the Laboratory for Laser Energetics, University of Rochester where he serves as Group Leader for X-Ray Devices. His research has been concerned with the development and applications of intense X-ray sources.

Dr. Forsyth received the Adolf Lomb Medal from the Optical Society of America in 1974 and was made a Fellow of OSA in 1978.

David M. Villeneuve was born in Ottawa, Ont., Canada, on April 19, 1952. He received the B.Math degree in 1975 and the Ph.D. degree in physics in 1980 from the University of Waterloo.

He was a postdoctoral fellow at the Laboratory for Laser Energetics, University of Rochester, Rochester, NY between 1980 and 1982. He is now with the Division of Physics, National Research Council, Ottawa, studying laser interaction with long scale length plasmas using Thomson scattering techniques.